Pergamon

International Journal of Machine Tools & Manufacture 42 (2002) 1055–1063

INTERNATIONAL JOURNAL OF
MACHINE TOOLS
& MANUFACTURE
DESIGN, RESEARCH AND APPLICATION

A method of modeling residual stress distribution in turning for different materials

M.H. El-Axir

Department of Production Engineering and Mechanical Design, Menoufia University, Shebin El-Kom, Egypt

Received 10 July 2001; received in revised form 7 March 2002; accepted 12 March 2002

Abstract

This paper introduces a more comprehensive experimental model which has the capability of predicting residual stress profile. The main advantage of this model over the existing models that it provides the effect of machining parameters on maximum residual stress and determines both the location and depth of this maximum residual stress. Five different materials namely; stainless steel-304, steel-37, 7001 and 2024-aluminum alloys and brass were machined by turning utilizing one of experimental design techniques based on response surface methodology. Tensile strength of these materials and both cutting speed and feed rates are considered as three input parameters affecting residual stress distribution. The residual stress distribution in the machined surface region was determined using a deflection-etching technique. It is proposed here that the residual stress profile is a deterministic function of the three input parameters used. Also, it is postulated that the residual stress profile along the depth beneath surface is a polynomial function of the depth beneath surface and the coefficients of this polynomial are, in turn, functions of the input parameters. The model has been developed and has been checked for accuracy. © 2002 Elsevier Science Ltd. All rights reserved.

Keywords: Residual stress modeling; Machining parameters; Aluminum alloys; Brass; Steel; Stainless steel

1. Introduction

Fatigue life is an important dynamic property and it is strongly affected by the surface condition produced during machining [1]. The fatigue crack, in general, nucleates at the surface of the part, and then propagates into the bulk. As the crack extends the resistant section is reduced, and when the residual section can no longer withstand the applied load component fatigue occurs. Consequently, it is the state of stress at the surface, where the crack nucleates, that is of paramount importance. This state is the sum of the stress due to the applied load and of the residual stresses (or self stresses) generated during machining. Residual stress is the result of various mechanical and thermal events, which occur in the surface region during machining. It is usually found that the absolute value of the residual stress close to surface it high and decreases continuously with an increase in depth beneath the machined surface eventually vanishing. Residual stress may be tensile or compressive and the stressed layer may be shallow or deep, depending upon the cutting conditions, work material, and tool geometry.

It has been shown [2–4] that residual stresses may be compressive at the surface and tensile just below the surface or vice versa. Compressive residual stresses are generally improve component performance and life because they reduce service (working) tensile stresses and inhibit crack nucleation. On the other hand, tensile residual stresses can significantly increase service (working) stresses which can lead to premature failure of components [5–10]. Sigwart and Fessenmeyer [11], for example, reported that fatigue tests on turned specimens of 42CrMo4 steel presenting high tensile residual stresses (up to 600:800 MPa) showed a close to 30% reduction in the fatigue limit. Matsumoto et al. [12] reported that the fatigue strength of hardened AISI 4340 steel specimens (54 HRC) after flycutting was 2–5% higher that after grinding probably because the compressive residual stress distribution produced by the single point cutting operation penetrated to a grater workpiece depth. Similarly, Prata Pina et al. [13] found that, when milling annealed hot work die steel (AISI H13),

E-mail address: ealaxir@yahoo.com (M.H. El-Axir).

0890-6955/02/$ - see front matter © 2002 Elsevier Science Ltd. All rights reserved.
PII: S0890-6955(02)00031-7

residual stresses close to zero were obtained at the surface, dropping sharply to a maximum compressive stress approximately 100 μm below the surface, then rising again to the tensile side.

Accordingly, It is very clear that the information concerning residual stresses profile (magnitude and direction along the depth) of the machined surface region will be valuable in the design and manufacture of parts. Therefore, it is important that the effect of the machining process parameters on the residual stress profile is determined, and subsequently, such machining parameters may be chosen which would enhance fatigue life by inducing favorable residual stress (compressive stress).

The majority of the research existing in literature on the effect of machining parameters on the residual stress profile are experimental in nature. Very few analytical models are available. Liu and Barash [14,15] explained the formation of residual stress by considering the stress strain history that the surface layer experienced due to the movement of the cutting tool. Lin et al. [9] used finite element techniques to determine residual stress profiles in orthogonal machining. Wu and Matusmoto [16] also used finite element to determine factors, which affect residual stress formation in hardened steel machining. Devarajan et al. [17] constructed an experimental model for prediction of the surface residual stress. Although the surface residual stress is important, in most machining processes, the subsurface residual stresses are at least equally important.

This paper introduces a more comprehensive experimental model to predict surface and subsurface residual stress profiles in turning of five different materials. With the help of this knowledge it will become possible to optimize machining parameters such that the surface integrity of the machined component for these five different materials is maximized under service conditions.

2. Experimental details

2.1. Workpiece materials

Workpieces of stainless steel 304, steel37, aluminum alloy 7001, aluminum alloy 2024, and brass were utilized. These materials were selected because they have different machining characteristics and are important in industry. Moreover, both of aluminum alloys 7001 and 2024 are particularly well suited for parts and structures requiring high strength-to-weight ratios. The chemical compositions in weight percent and tensile strength are given in Table 1. The tool material employed was high-speed steel.

2.2. Workpiece preparation

The five different materials were machined into ring shapes with the dimensions shown in Fig. 1a. Fig. 1b shows the tested ring mounted on its mandrel. It is probable that residual stresses are induced in the surface region of the workpiece because of the machining involved in preparation, hence it was necessary to remove these stresses by annealing the workpieces.

Stainless steel 304, steel 37, Al. 7001, Al. 2024 and free machining brass workpieces were heated to 800, 595, 340, 340, and 260°C for 3, 6, 2, 2 and 1 h, respectively, and then cooled in air or in furnace.

In this investigation, the specimens were machined using one of the experimental designs. According to a central composed second-order rotatable design with three independent variables, the total number of experiments, N, was determined to be 20. The cutting conditions and their coded are summarized in Table 2.

The residual stress distribution in the machined surface was determined utilizing a deflection etching technique where the residual stresses in the removal layer are relived and the remaining residual stresses are redistributed until a new equilibrium position is achieved. This change in shape can be measured from which residual stresses can be calculated. A layer of approximately 15–25 μm was removed with the help of electrochemical etching. Layers were removed until the residual stress state became negligible. The obtained residual stress profiles for 20 different combinations according to Table 3 are shown in Fig. 2.

3. Proposed model

The proposed model postulates that the residual stress profile as well as the depth of residual stress distribution are functions of the machining parameters. The model assumes that profile of residual stress along the depth is polynomial function of the depth. The profile can be represented as:

$$\sigma_i = c_{oi} + c_{1i}z + c_{2i}z^2 + c_{2i}z^3 + \ldots + c_{ni}z^n$$

where: σ_i is the residual stress, c_{ni} are the coefficients of the nth order polynomial term and z is the depth beneath the machined surface.

Further, it is proposed that the coefficients of the polynomial are individual functions of the machining parameters. The relation of the coefficient to the machining parameters is

$$c_i = b_{oi} + b_{vi}v + b_{fi}f + v_{ti}t + b_{vfi}vf + b_{vti}vt + b_{fti}ft\ldots \quad (1)$$

where C_i is the coefficient of polynomial for residual stress profile and b_{xi} is the effect of factor (or interaction of factor) x.

The values of the code number of each parameter, x, can be obtained from the following transformation equations.

Table 1
Chemical composition of workpiece materials in weight percent

Material	Chemical composition								
	C	Si	Mn	P	S	Cr	Ni	Fe	
Stainless steel(304)	0.08	1.0	2.00	0.045	0.03	18–20	8–10	Balance	
Steel-37	0.2			0.08	0.05				
Al. alloy	Cu	Mn	Mg	Cr	Ni	Zn	Fe	Pb	Al
2024	4.4	0.6	1.5		2				Balance
7001	2.1		3.0	0.3		7.4	0.5		Balance
Brass	57.68					40.287	0.043	1.99	
	Tensile strength (MPa)								
S-S 304	615								
Steel 37	490								
AL 2024	177								
AL 7001	360								
Brass	255								

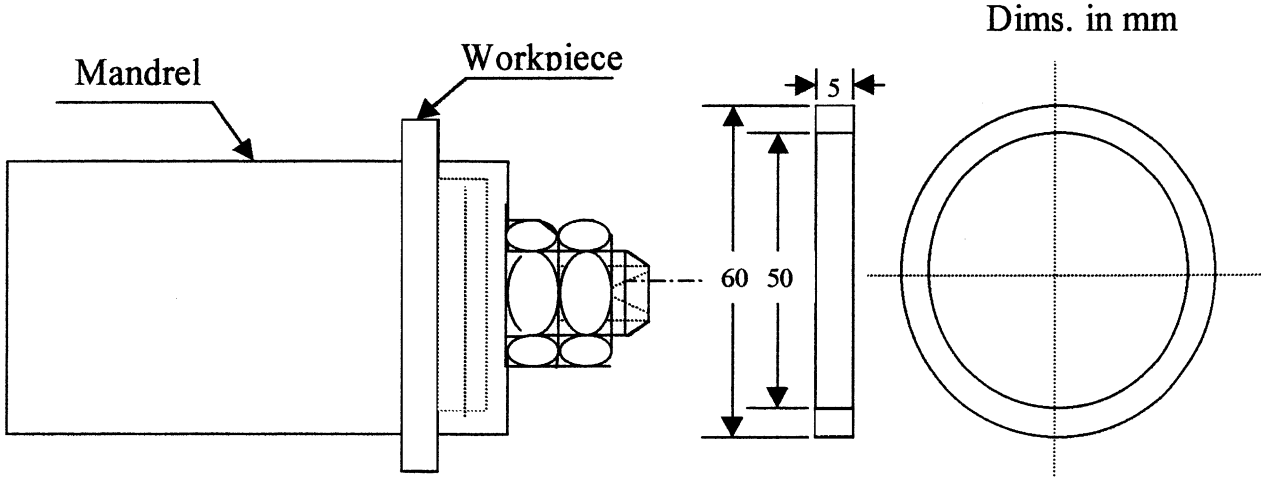

Fig. 1. Mandrel and workpiece.

Table 2
Summary of machining conditions

Parameters	Symbol	Levels in code form				
		Lowest	Low	Center	High	Highest
Cutting speed, m/sec	$X1$	0.236	0.467	0.93	1.88	3.77
Feed, mm/rev	X_2	0.025	0.05	0.10	0.2	0.4
Tensile strength kg/mm^2	$X3$	177	255	360	490	615

Cutting speed

$$x_1 = \frac{2(\log V - \log V_{+1})}{\log V_{+1} - \log V_{-1}} + 1 \quad (2)$$

Feed rate

$$x_2 = \frac{2(\log F - \log F_{+1})}{\log F_{+1} - \log F_{-1}} + 1 \quad (3)$$

Tensile strength

$$x_3 = \frac{2(\log T - \log T_{+1})}{\log T_{+1} - \log T_{-1}} + 1 \quad (4)$$

where V, F and T are cutting speed, feed and tensile strength of the material, respectively.

The values of b_{xi}s are determined experimentally. The procedure is as follows:

1. Twenty specimens are cut using different combinations (Table 3) of the five levels of each parameter used in this work.
2. The residual stress profiles and depth of distribution for each specimen are determined.
3. Polynomials of a pre-decided degree are fitted to the residual stress profiles for each specimen.

Table 3
Experimental design matrix

Combination No.	Input parameters					
	Cutting speed		Feed rate		Tensile strength	
1	(−1)	Low	(−1)	Low	(−1)	Low
2	(+1)	High	(−1)	Low	(−1)	Low
3	(−1)	Low	(+1)	High	(−1)	Low
4	(+1)	High	(+1)	High	(−1)	Low
5	(−1)	Low	(−1)	Low	(+1)	High
6	(+1)	High	(−1)	Low	(+1)	High
7	(−1)	Low	(+1)	High	(+1)	High
8	(+1)	High	(+1)	High	(+1)	High
9	(−1.682)	Lowest	(0)	Center	(+1)	Center
10	(+1.682)	Highest	(0)	Center	(0)	Center
11	(0)	Center	(−1.682)	Lowest	(0)	Center
12	(0)	Center	(+1.682)	Highest	(0)	Center
13	(0)	Center	(0)	Center	(−1.682)	Lowest
14	(0)	Center	(0)	Center	(+1.682)	Highest
15	(0)	Center	(0)	Center	(0)	Center
16	(0)	Center	(0)	Center	(0)	Center
17	(0)	Center	(0)	Center	(0)	Center
18	(0)	Center	(0)	Center	(0)	Center
19	(0)	Center	(0)	Center	(0)	Center
20	(0)	Center	(0)	Center	(0)	Center

4. The coefficient (r_{li}) of these polynomials are then used to determine the values of b_{xi}s with the help of the following expressions:

$$b_{oi} = r_{1I} + r_{2I} + r_{3I} + r_{4I} + r_{5I} + r_{6I} + r_{7I} + r_{8I} + \ldots r_{20I}$$

$$b_{vi} = -r_{1I} + r_{2I} - r_{3I} + r_{4I} - r_{5I} + r_{6I} - r_{7I} + r_{8I} + \ldots r_{10i}$$

$$b_{fi} = -r_{1I} - r_{2I} + r_{3I} + r_{4I} - r_{5I} - r_{6I} + r_{7I} + r_{8I} + \ldots r_{12i}$$

$$b_{ti} = -r_{1I} - r_{2I} - r_{3I} - r_{4I} + r_{5I} + r_{6I} + r_{7I} + r_{8I} + \ldots r_{14i}$$

$$b_{vfi} = r_{1I} - r_{2I} - r_{3I} + r_{4I} + r_{5I} - r_{6I} - r_{7I} + r_{8I}$$

$$b_{vti} = r_{1I} - r_{2I} + r_{3I} - r_{4I} - r_{5I} + r_{6I} - r_{7I} + r_{8I}$$

$$b_{fbi} = r_{1I} + r_{2I} - r_{3I} - r_{4I} - r_{5I} - r_{6I} + r_{7I} + r_{8I}$$

4. Construction of the proposed model

A visual inspection of the profiles obtained warranted that at least a fourth degree polynomial would be regarded as sufficient to fit the profile. Preliminary results with a fourth degree polynomial were not encouraging. Therefore, it was decided to use fifth degree polynomial to represent the residual stress profile. The coefficients (r_{li}s) corresponding to the closest fit with fifth degree polynomial for different combinations are shown in Table 4.

It should be pointed out here that many attempts were carried out to deduce the best model that gives the smallest variation between the fitted polynomial and the proposed model results. The best method that gives simple and reasonable coefficients was obtained when the normalized value of each experimented result was used.

Using the coefficient of fit polynomial equation of each experiment, the values of b_{xi}s were determined. The calculated values of b_{xi}s are shown in Table 5. The b_{xi}s were used to predict c_is which are the coefficients of the proposed model. The values of c_is for various cutting conditions are shown in Table 6.

4.1. How the proposed model is used

To show how the proposed model is used and also to verify the proposed model, two extra tests that were not conducted through the 20 experiments, were made. The results of those two extra tests are shown in Fig. 4 which indicate a good agreement between the experiments data and proposed model data. This proves the validity of using the proposed model to predict the distribution of residual stress beneath the machined surface. Steps that would be followed to use the proposed model to predict the distribution of residual stress beneath the machined surface are shown in Tables 4–6.

4.1.1. Step 1

Transfer the value of the three input parameters to coded value using the transformation eqs. (2)–(4). In the two extra tests, the actual and coded values are:

Test I		Test II	
Actual value	Coded value	Actual value	Coded value
Cutting speed, V=117m/min	$x_1 = 1.0529$	Cutting speed, V=171m/min	$x_1 = 1.598$
Feed, f=0.356	$x_2 = 1.4176$	Feed, f=0.2mm/rev	$x_2 = 1.000$
Tensile strength=360 MPa	$x_3 = 0$	Tensile strength=360 MPa	$x_3 = 0$

4.1.2. Step 2

The c coefficients in the proposed model should be calculated by using the coded values of the three input parameters that were obtained in step 1 and using the b values that are shown in Table 5.

$$\sigma_i = c_{oi} + c_{1i}z + c_{2i}z^2 + c_{3i}z^3 + \ldots + c_{ni}z^n \quad (5)$$

For example: the coefficient C_o can be obtained using the b values from Table 5 as follows:

$$C_o = -020749 + 0.2151017*X_1 + 0.051308*X_2$$

Table 4
Coefficients of fifth polynomial fitted to data obtained in experiments according to experimental design matrix

Combination No.	Coefficients of experimentally determined polynomial (r_{li})					
	0	1	2	3	4	5
1	−0.3989	−0.4473	−0.0326	0.0703	0.1279	−0.0145
2	−0.7185	−0.2849	0.3506	0.5728	2.4616	−1.6828
3	−0.3529	−0.3768	−0.0599	−1.4299	−0.0015	1.1729
4	−0.4594	−1.5260	3.2860	−1.4448	−1.8840	0.3978
5	0.1192	−2.6944	3.4264	−0.8710	−1.0440	−0.3978
6	0.7055	−3.1887	3.2481	−0.0655	−1.2518	−0.3043
7	0.0125	−1.8353	1.0206	0.4785	2.6531	−3.3055
8	0.1283	−1.1254	−1.6964	1.1085	6.3314	−5.8612
9	−0.5392	−0.7922	0.9310	−1.2681	0.1922	0.7352
10	0.5764	−2.9870	1.0510	0.8050	1.1922	−1.3572
11	−0.2333	−0.4115	0.3491	−3.0925	1.2745	1.7352
12	0.2957	−1.2949	−0.7300	−1.752	3.9480	−4.9324
13	−0.8070	0.4280	−0.4981	−0.1637r	2.4658	−0.3689
14	−0.8060	−1.4660	5.0400	−5.1160	−0.4420	1.7231
15	−0.6370	−1.0950	0.7345	0.9470	0.5897	−1.8081
16	−0.8880	−0.2760	2.2300	−2.5800	−2.2900	4.0400
17	−0.7897	−0.6770	3.3280	−3.3600	−3.4000	5.2830
18	−1.0190	−0.0050	3.7700	−5.2200	−3.6300	4.4540
19	−0.8780	−0.4980	3.4300	−3.8800	−3.5400	8.0780
20	−0.8320	−0.0273	3.4040	−7.1600	−1.6700	−0.7203

Table 5
Calculated values of b_{xi}

Factor or interaction (x)	Effect of x (b_{xi}) on coefficient (I)					
	0	1	2	3	4	5
O	−0.207490	−1.273230	1.094687	−0.748280	1.107773	−0.720320
V	0.215017	−0.446290	0.103564	0.541005	0.559835	0.501514
F	0.051308	0.026424	−0.625720	−0.126513	1.130193	0.611742
M	0.281828	−0.934850	1.171987	−0.546400	0.134056	0.244117
Vf	−0.032144	−0.013430	0.053000	0.086610	−0.04129	−0.144030
Vm	0.140763	0.150300	−0.838050	0.118488	0.377438	−0.189150
Fm	−0.12336 0	0.511625	−1.282300	0.755163	1.969388	−1.017000

Table 6
Predicted values of C_i

Combination No.	Coefficients of experimentally determined polynomial (r_{ii})					
	0	1	2	3	4	5
1	−0.64732	0.72999	−1.61249	−0.08236	1.58923	−3.42787
2	0.43394	−0.43633	0.14474	0.93590	2.03659	−1.75849
3	−0.47983	−0.21356	−0.40534	−1.16643	−0.00659	0.11766
4	−0.39620	−1.43358	1.56389	−0.49462	0.27563	1.21094
5	−0.36519	−2.46357	4.95218	−2.92246	−2.83631	−0.52723
6	0.41124	−3.02869	3.39721	−1.43025	−0.87919	−0.38545
7	−0.19770	−1.36062	1.02301	−0.98589	1.47604	−1.04980
8	0.44898	−1.97944	−0.63128	0.15987	5.23739	−0.71312
9	−0.69150	−0.52257	0.93049	−1.65825	0.16613	−1.56387
10	0.15416	−2.02388	1.26888	0.16169	2.04942	0.12323
11	−0.29379	−1.31767	2.14716	−0.96107	−0.79321	−1.74927
12	−0.12119	−1.22878	−0.42218	−1.53549	3.00876	−0.30862
13	−0.65335	0.20571	−0.75940	−0.11613	1.46580	−0.16890
14	−0.26654	−2.44565	3.06597	−1.88733	0.33326	−0.30972
15	−0.63700	−1.09500	0.73450	0.94700	0.58970	−1.80810
16	−0.63700	−1.09500	0.73450	0.94700	0.58970	−1.80810
17	−0.63700	−1.09500	0.73450	0.94700	0.58970	−1.80810
18	−0.63700	−1.09500	0.73450	0.94700	0.58970	−1.80810
19	−0.63700	−1.09500	0.73450	0.94700	0.58970	−1.80810
20	−0.63700	−1.09500	0.73450	0.94700	0.58970	−1.80810

$$+ 0.28128*X_3 - 0.032144*X_1*X_2 + 0.14076*X_1*X_3 - 0.12336*X_2*X_3$$

The value of the *c* coefficients of the two extra tests are shown in Table 7.

4.1.3. Step 3

After obtaining the *c* values, eq. (5) that is a function in depth beneath surface, *z*, could be formed and the residual stress distribution beneath the machined surface can be determined. However, before substituting in this equation, the value of the depth beneath surface, *z*, must be transferred to a normalized value.

4.1.4. Step 4

By substituting in the σ equation using any depth, *z*, the residual stress at this depth can be obtained. It should be pointed out here that this obtained residual stress is normalized. The latter value of residual stress has to be transferred to the actual value by the following equations. The material used in the two extra tests was Al-7001 (the third relationship should be used).

For brass $\sigma_{(\text{actual})} = \sigma_{(\text{normalized})}*65 + 65$
For steel and stainless steel $\sigma_{(\text{actual})} = \sigma_{(\text{normalized})}*50 + 50$
For Al-7001 $\sigma_{(\text{actual})} = \sigma_{(\text{normalized})}*60 + 60$
For Al-2024 $\sigma_{(\text{actual})} = \sigma_{(\text{normalized})}*45 + 45$

4.1.5. Step 5

The surface stresses were calculated using a separate model. This was made because at workpiece surface, the residual stress is small and suddenly reaches a maximum value at 20–40 μm beneath the surface which loosen the accuracy of the derived model.

The surface residual stress model that was used to predict the value of residual stress in the machined surface at any value of each parameter within the range used in this work is as follows:

$$\sigma surface = 18.425 + 0.769v + 5.14f + 26.2m + 3.125vf + 24.3vm + 13.125fm, \quad (6)$$

Where *v*, *f*, *m* are the cutting speed, feed, and tensile strength of workpiece material respectively, after being transferred to the coded value using the equation.

In the extra two tests, the surface residual stress that were obtained using eq. (6) are 30.0871 and 32.485 MPa, respectively.

5. General discussion and summary

It can generally be seen from Fig. 2 that the residual stresses at the machined surface are low (tensile) and increase rapidly to a maximum (tensile) value with an increase in depth beneath the machined surface. The tensile residual stresses then decrease gradually with a further increase in depth beneath the machined surface.

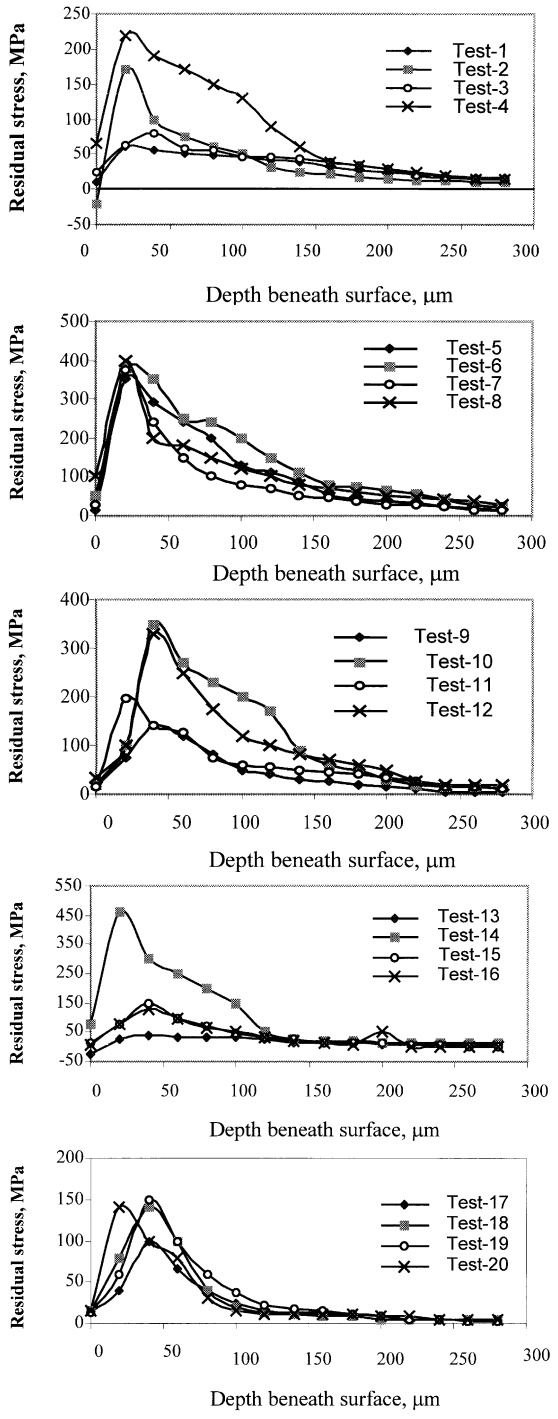

Fig. 2. Residual stress profiles measured from the machined surface.

Complete analysis of the data showed that the residual stress continued to decrease across the section become either tensile or compressive at large depths. The maximum residual stresses always occur beneath the machined surface rather than on the nearest layer to the machined surface. The underlying assumption in the entire model is that residual stress produced by identical conditions is also fairly identical. The variability of the profiles could be checked with standard variance techniques, but for this paper, a visual check was deemed sufficient.

Models with the capability of predicting residual stresses in machining operations are the critical link in the development of more complex models which can enable the concept of 'custom manufacture' machining of stainless steel, steel, aluminum alloy, brass. Once such models are known, they can be used in conjunction with other models to provide information about the residual stress profile that would be most favorable in service conditions, and the used materials can be machined to maximize fatigue life.

In this paper an experimental model is described which has the capability of predicting residual stresses in five different materials as result of turning operations. The proposed model fitted the experimental data with a high degree of accuracy as shown in Fig. 3. It should be pointed out here that this paper concentrates only on modeling the effect of machining parameters on residual stress distribution.

References

[1] M. Fied, J.F. Kahles, J.T. Cammett, A review of measuring methods for surface integrity, Ann. CIRP 21 (2) (1972) 219–238.
[2] S. Mittal, C.R. Lid, A method of modeling residual stresses in superfinish hard turning, Wear 218 (1998) 21.
[3] I.C. Noyan, J.B. Cohen, The nature of residual stress and its measurement, Sagamore Army Material Research Conference Proceedings 28 (1981) 1.
[4] C.R. Liu, M.M. Barash, Variable governing patterns of mechanical residual stress in a machined surface. ASME, Paper No.82-WA/Prod-8 (1982).
[5] J.D. Thiele, S.N. Melkote, R.A. Peascoe, T.R. Watkins, Effect of cutting-edge geometry and workpiece hardness on surface residual stresses in finish hard turning of AISI 0 steel, J. Manufacturing Science and Engineering 122 (2000) 642.
[6] K. Huafuh, W. Chih-Fu, A residual-stress model for the milling of aluminum alloy (2014-T6), J. Material Processing Technology 51 (1995) 87.
[7] M.H. El-Axir, J.A. Bailey, M.M. El-Khabeery, Effects of selected cutting parameters on fatigue life, maximum residual stress, and surface roughness: Part—I unlubricated conditions, in: Second Assiut University Int. Conf. Mech. Eng. Advanced Tech. for Industrial Production, 1999, 2–4 March, pp. 306–318.
[8] M.H. El-Axir, J.A. Bailey, M.M. El-Khabeery, Effects of selected cutting parameters on fatigue life, maximum residual stress, and surface roughness: Part—II lubricated conditions, in: Second Assiut University Int. Conf. Mech. Eng. Advanced Tech. for Industrial Production, 1999, 2–4 March, pp. 319–327.
[9] Z-C. Lin, Y-Y. Lin, C.R. Liu, Effect of thermal load and mechanical load on the residual stress of a machined workpiece, Int. J. Mech. Sci. 33 (4) (1991) 263–278.
[10] M.M. Elkhabeery, M. Fattoh, Residual stress distribution caused by milling, Int. J. Mach. Tools Manufact. 29 (3) (1989) 391.
[11] A. Sigwart, W. Fessenmeyer, Oberflache und Randschicht. VDI Berichte 1227, VDI Verlag, 1995.
[12] Y. Matsumoto, D. Magda, D.W. Hoeppner, T.Y. Kim, Effect of machining processes on the fatigue strength of hardened AISI-steel, J. Eng. Ind. 13 (1991) 154–159.
[13] J. Prata Pina, A. Morao Dias, J.L. Lebrun, Study of residual

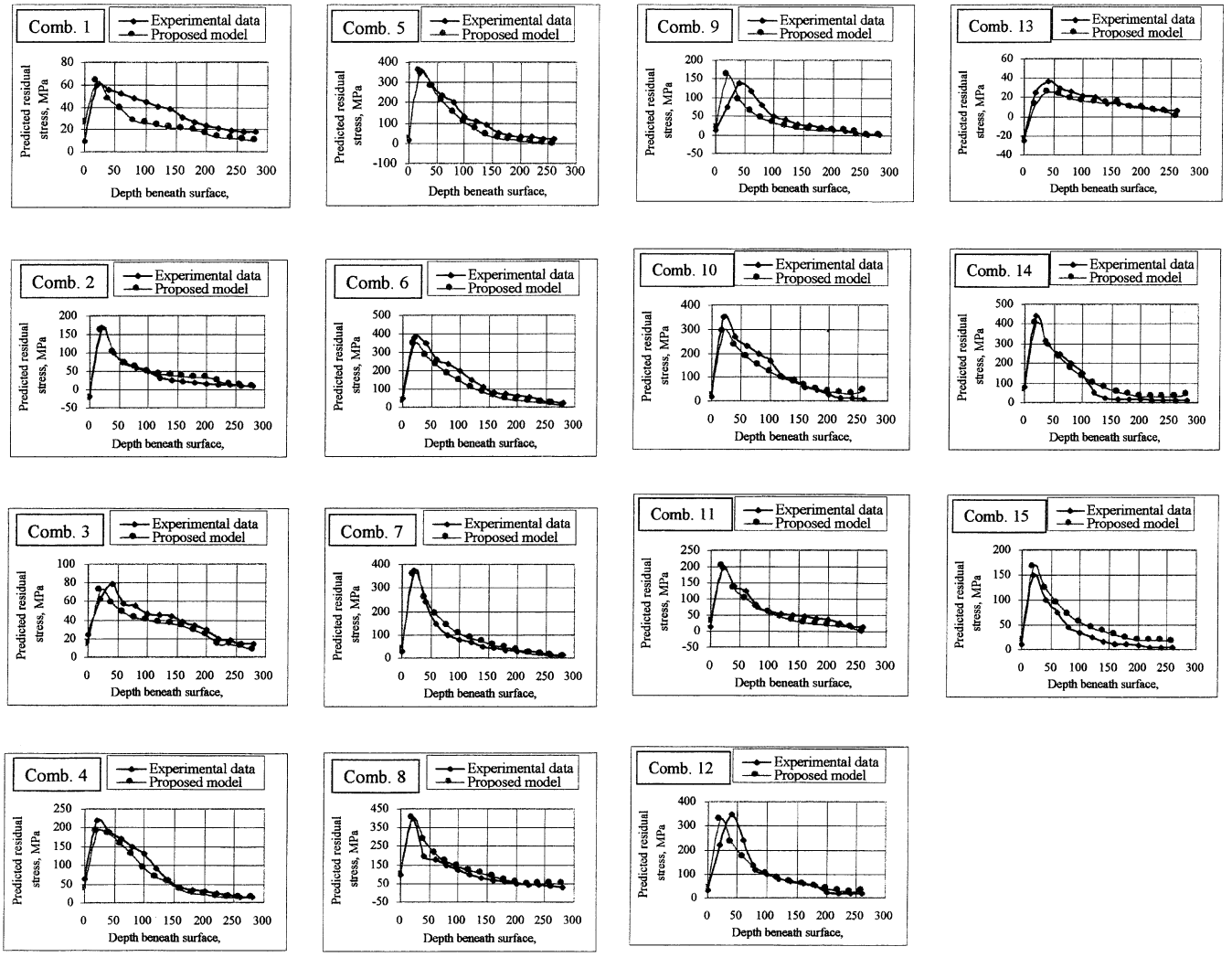

Fig. 3. Experimental data of residual stress profiles and residual stress profiles predicted by the proposed model.

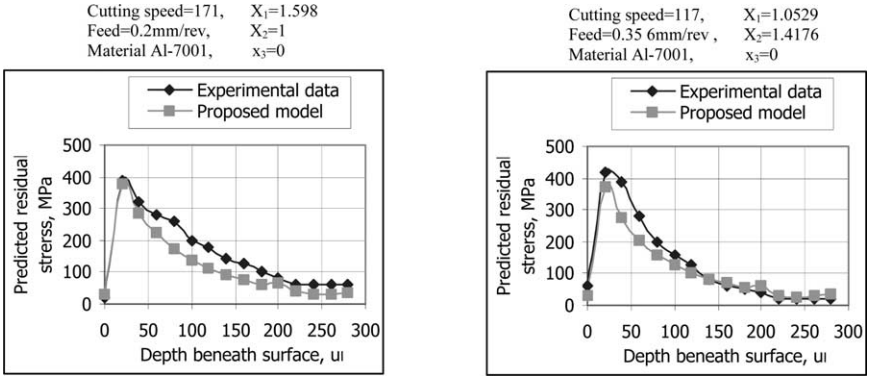

Fig. 4. Comparison of experimental and proposed model data — validation trials.

Table 7
C values of the two extra tests

C's coefficient	C_0	C_1	C_2	C_3	C_4	C_5
Test I	0.136049	−1.98144	0.634462	0.127836	3.066601	0.692841
Test II	0.043658	−1.72572	0.316709	−0.22903	3.237756	0.67493

stresses and cold working generated by machining of AISI H13 steel, in: Int. Conf. on Residual Stresses, ICR2, Nancy, France.
[14] C.R. Liu, M.M. Barash, The mechanical state of the sublayer of a surface generated by chip-removed process parts 1 and 2, J. Eng. Ind. 98 (4) (1976) 1195–1208.
[15] C.R. Liu, M.M. Barash, Variables governing patterns of mechanical residual stress in a machined surface, in: Technical Report 82-prod.-8, ASME, New York, 1982.
[16] S.W. Wu, Y. Matsumoto, The effect of hardness on residual stresses in orthogonal machining of AISI steel, J. Eng. Ind. 112 (1990) 245–252.
[17] N. Devarajan, M.K. Asundi, S. Somasundaran, Experimental method for predicting residual stresses due to turning in stainless steel, Exp. Tech. 8 (1984) 22–26.